J. Cent. South Univ. (2015) 22: 2503−2507
DOI: 10.1007/s11771-015-2778-1

Springer

Effects of minerals in ferric bauxite on sodium carbonate decomposition and volatilization

HU Wen-tao(胡文韬)[1], WANG Hua-jun(王化军)[1], LIU Xin-wei(刘欣伟)[1], SUN Chuan-yao(孙传尧)[1, 2]

1. Key Laboratory of High-Efficient Mining and Safety of Metal Mines (USTB) of Ministry of Education (University of Science and Technology Beijing), Beijing 100083, China;
2. State Key Laboratory of Mineral Processing Science and Technology (Beijing General Research Institute of Mining and Metallurgy), Beijing 100070, China;

Abstract: Direct reduction is an emerging technology for ferric bauxite utilization. However, because of sodium volatilization, its sodium carbonate consumption is considerably higher than that in ordinary bauxite processing technology. TG-DSC and XRD were applied to detecting phase transformation and mass loss in direct reduction to reveal the mechanism on sodium volatilization. The results show that the most significant influence factor of ferric bauxite on sodium volatilization in direct reduction system is its iron content. Sodium volatilization is probably ascribed to the instability of amorphous substances structure. Amorphous substances are the intermediate-products of the reaction, and the volatilization rate of sodium increases with its generating rate. These amorphous substances are volatile, thus, more sodium is volatilized with its generation. A small amount of amorphous substances are generated in the reaction between Na_2CO_3 and Al_2O_3; thus, only 3.15% of sodium is volatilized. Similarly, the volatilization rate is 1.87% in the reaction between Na_2CO_3 and SiO_2. However, the volatilization rate reaches 7.64% in the reaction between Na_2CO_3 and Fe_2O_3 because of the generation of a large amount of amorphous substances.

Key words: Na_2CO_3 decomposition; Na_2CO_3 volatilization; ferric bauxite; direct reduction

1 Introduction

Ferric bauxite, a type of bauxite with high hematite content, has yet to be commercialized. Direct reduction [1−2] can realize ferric bauxite comprehensive utilization; however, the sodium carbonate consumption in direct reduction is considerably higher than that in the ordinary bauxite processing technology [3]. Previous research indicated that sodium carbonate consumption is caused by sodium volatilization [2−5]. This volatilization is nondirectional, allowing it to become a new unorganized alkali pollutant source. Ferric bauxite and ordinary bauxite principally differ in their mineral compositions. Therefore, the decomposition and volatilization of sodium carbonate can be promoted by a certain chemical composition of ferric bauxite. Ferric bauxite is mainly composed of SiO_2, Al_2O_3, and Fe_2O_3. NEWKIRK and ALIFERIS [6] found that silica can promote the volatilization and decomposition of sodium carbonate. However, the effect of Al_2O_3 and Fe_2O_3 on the volatilization and decomposition of sodium carbonate remains unclear. In addition, the volatilization mechanism research conducted by NEWKIRK and ALIFERIS [6] was mainly focused on the weightlessness of reactants and rarely on the phase change in the weightlessness process. X-ray diffraction (XRD) [7−11] and thermogravimetry (TG)-differential scanning calorimetry (DSC) [12−16] have been widely applied in mineralogy research. In the present work, the effects of SiO_2, Al_2O_3 and Fe_2O_3 on sodium volatilization were investigated by TG-DSC. The phase change in the heating process was studied by XRD. This work aims to determine the effects of the three main components in ferric bauxite on the volatilization and decomposition of sodium and to elucidate the phase change and heat adsorption mechanism in sodium carbonate volatilization.

2 Materials and methods

2.1 Raw materials

The simulated ferric bauxite was supplied by Guangxi Zhuang Autonomous Region of China. The chemical analysis result of the ore is given in Table 1. The XRD pattern is shown in Fig. 1.

Foundation item: Project(51304012) supported by the National Natural Science Foundation of China; Project(2014M550845) supported by China Postdoctoral Science Foundation; Project(KF13-05) supported by Open Foundation of the State Key Laboratory of Advanced Metallurgy (USTB), China
Received date: 2014−06−17; **Accepted date:** 2014−10−20
Corresponding author: WANG Hua-jun, Professor, Tel: +86−10−62332902; E-mail: wanghuajun@bjjzq.com

Table 1 Main chemical composition of ore (mass fraction, %)

Fe_2O_3	Al_2O_3	SiO_2	TiO_2	MgO
41.13	33.02	12.22	1.49	0.68
CaO	Na_2O	K_2O	P_2O_5	Ignition loss
0.63	0.32	0.06	0.04	8.97

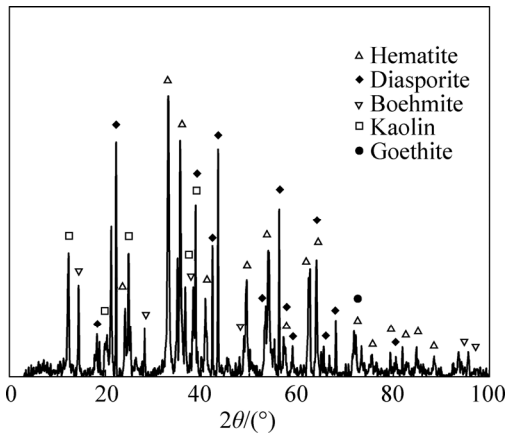

Fig. 1 XRD pattern of ferric bauxite ore

Combining the chemical composition and the XRD pattern, we calculated the mineral composition of Al-bearing minerals as 68.54% diaspore (or boehmite) and 31.46% clay.

Pure minerals are difficult to find; hence, substitutes were used. Both diaspore and boehmite were decomposed into corundum at 800 °C [5]. Thus, corundum was used as a substitute for diaspore and boehmite. Similarly, the main structural unit of kaolinite contains silicon-oxygen tetrahedron and aluminum-oxygen octahedron, and quartz and corundum in molten state exist in the form of silicon-oxytetrahedron or aluminum-oxygen octahedron. Thus, quartz and corundum were used as substitutes for kaolinite. These substitutes were not in their normal mineral phase after heating. Therefore, they were shown as Fe_2O_3, Al_2O_3, and SiO_2, and sodium carbonate was shown as Na_2CO_3. The raw materials used in the experiment are given in Table 2.

Proximate analysis data of the coal used are given in Table 3. The multi-element analysis data of the coal ash content are given in Table 4.

Table 2 List of raw materials

Reagent	Purity	Producer
Na_2CO_3	AR	Beijing Chemical Works (China)
Al_2O_3	AR	Guangdong Xilong Chemical Industry Co. (China)
SiO_2	AR	Guangdong Xilong Chemical Industry Co. (China)
Fe_2O_3	AR	Tianjin No. 3 Chemical Reagent Factory (China)

Table 3 Proximate analysis data of coal (mass fraction, %)

Total moisture	Volatile content	Ash content	Fixed carbon
9.16	39.42	5.07	46.35

Table 4 Multi-element analysis data of ash content (mass fraction, %)

SiO_2	Al_2O_3	TFe	MgO	CaO
38.0	21.37	15.8	1.90	7.15
Na_2O	K_2O	TiO_2	P_2O_5	
0.43	1.38	0.84	0.41	

2.2 Experimental procedures

2.2.1 Preparation of mixture materials

Al_2O_3, SiO_2 or Fe_2O_3 was mixed with Na_2CO_3 at a molar ratio of 1:1 to determine their individual effects on Na_2CO_3 volatilization. The materials were mixed by using a planetary ball mill for 24 h, during which ethanol was added to enhance the dispersion of mineral particles.

2.2.2 TGA of mixtures

A TA Q600 (manufactured by TA in America) TG-DSC system was used to determine the TG and DSC experimental points of the mixtures at the same heating rate. A given amount of each mixture sample was placed in a platinum crucible, and its mass loss was recorded at a heating rate of 10 °C/min in N_2 atmosphere, with a carrier gas flow rate of 100 mL/min. The thermoanalysis standards were ASTM E2402 — 2005 and ASTM E2550—2007.

2.2.3 Crucible ancillary test

Direct reduction experiments of the mixture materials were conducted at different temperatures in a tube furnace, in which the heating environment was set the same as that in the thermal analyzer, to study the phase transformation of mixture materials in the thermal analysis process. The mineralogical composition of the mixture materials after direct reduction at different temperatures was determined by XRD analysis (Rigaku, Model-RH 200, Japan) at a scanning rate of 2 (°)/min with Cu K_α radiation.

2.2.4 Evaporative sodium

In this work, we mainly discussed the amount of evaporative sodium rather than the sodium evaporated. Hereinafter, the sodium mentioned represents an element.

3 Results and discussion

3.1 Effects of Al_2O_3

The reaction between Na_2CO_3 and Al_2O_3 can be written as

$$Al_2O_3 + Na_2CO_3 = Al_2O_3 \cdot Na_2O + CO_2 \uparrow \quad (1)$$

The TG and DSC curves of the Na_2CO_3-Al_2O_3 mixture are shown in Fig. 2, and the XRD patterns of the reaction products at different temperatures (30, 600, 700, 950 and 1165 °C) are shown in Fig. 3.

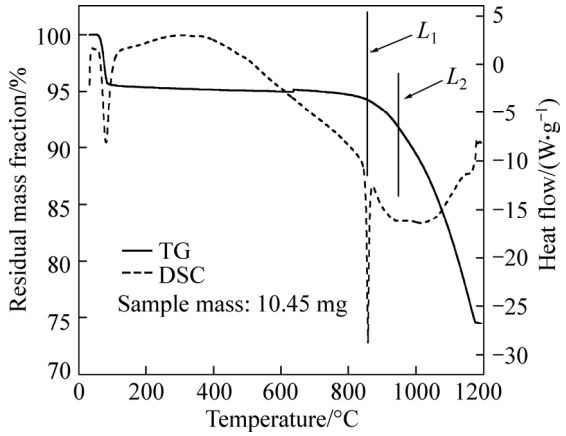

Fig. 2 TG and DSC curves of Na_2CO_3-Al_2O_3 mixture

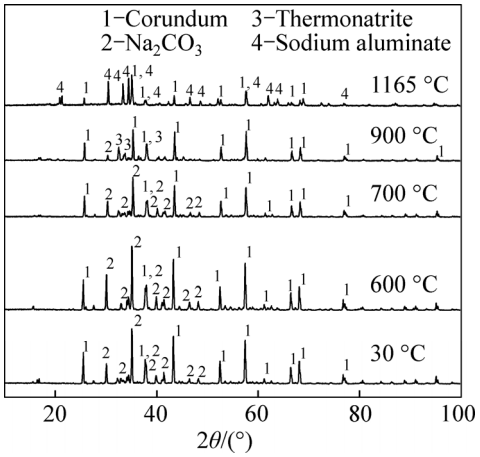

Fig. 3 XRD patterns of heated products of Na_2CO_3-Al_2O_3 mixture

In Fig. 2, L_1 represents 856.05 °C. At the beginning of the Na_2CO_3 endothermic progress at 856.05 °C, the endothermic peak is not accompanied by obvious mass loss. This result indicates that the endothermic peak is caused by the fusion rather than the decomposition of Na_2CO_3. However, rapid mass loss is detected above 856.05 °C, as shown in the TG curve in Fig. 2. At this point, Na_2CO_3 is melted. This result indicates that the chemical reaction between the two reactants mainly occurs in the fusion and not in the solid state. The TG curve in Fig. 2 shows that the mass loss is finished at 1174.91 °C, where the residual mass ratio is 74.64%. However, if the mass loss is only caused by CO_2 overflow, the theoretical value of the residual mass ratio should be 75.50%. Therefore, the rest of mass loss can only be caused by sodium volatilization, and the volatilization rate is 3.15%.

In Fig. 2, L_2 represents 950 °C. The TG curve in Fig. 2 shows that the mass loss begins to appear before 856.05 °C, suggesting that Na_2CO_3 has already started to decompose at 950 °C. However, no diffraction peak of the reaction product is observed in Fig. 3. This result suggests that the reaction product is present in amorphous form.

CO_2, the gaseous product of sodium carbonate decomposition, can be removed by nitrogen flow. Therefore, the decomposition of sodium carbonate reaction can be carried out completely [2]. In conclusion, only a small amount of amorphous substances is generated in the reaction progress, and only 3.15% of sodium is evaporated.

3.2 Effects of SiO_2

The TG and DSC curves of the Na_2CO_3-SiO_2 mixture are shown in Fig. 4. The reaction between SiO_2 and Na_2CO_3 can be written as Eq. (2). The XRD patterns of the heated products at different temperatures (30, 600, 700, 830, 950 and 1165 °C) are shown in Fig. 5.

$$SiO_2 + Na_2CO_3 = SiO_2 \cdot Na_2O + CO_2 \uparrow \quad (2)$$

As shown in Fig. 5, the Na_2SiO_3 diffraction peak disappears in the range of 950−1165 °C. However, no new substance is formed. Therefore, the endothermic

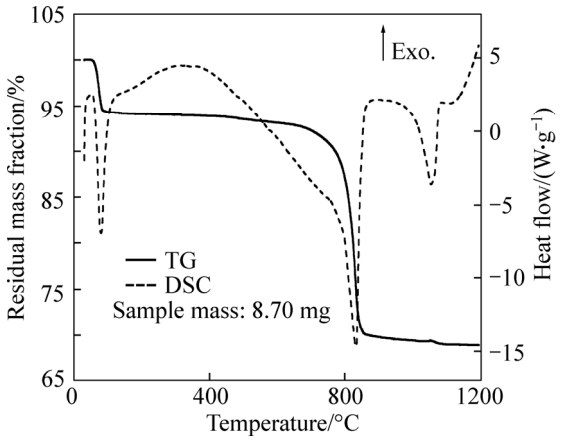

Fig. 4 Thermal analysis curves of Na_2CO_3-SiO_2 mixture

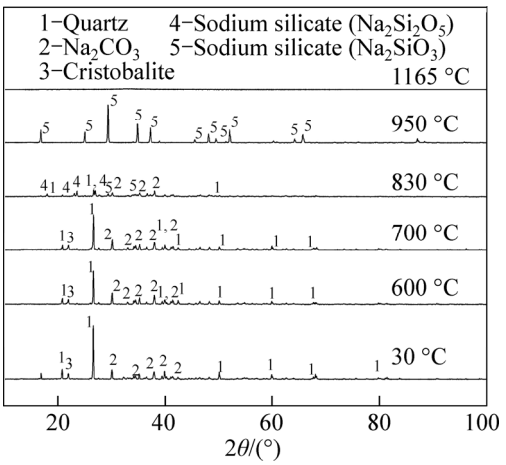

Fig. 5 XPD patterns of heated products of Na_2CO_3-SiO_2 mixture

peak at 1052.93 °C in Fig. 4 can only be caused by Na_2SiO_3 melting. As shown in Fig. 5, $Na_2Si_2O_5$ and Na_2SiO_3, generated after heating the SiO_2-Na_2CO_3 mixture, are crystallines. Hence, almost no amorphous substance is generated in the reaction process. The TG curve in Fig. 4 shows that the mass loss is finished at 1199.82 °C, where the residual mass ratio is 68.86%. This ratio is lower than the theoretical value, and the rest of the mass loss can only be caused by sodium volatilization. Thus, the sodium volatilization rate of the SiO_2-Na_2CO_3 mixture is calculated to be 1.87%.

3.3 Effects of Fe_2O_3

The TG and DSC curves of the Na_2CO_3-Fe_2O_3 mixture are shown in Fig. 6. The reaction can be written as

$$Fe_2O_3 + Na_2CO_3 = Fe_2O_3 \cdot Na_2O + CO_2 \uparrow \quad (3)$$

The XRD patterns of the reaction products at different temperatures (30, 600, 700, 850 and 950 °C) are demonstrated in Fig. 7.

According to the study results in Sections 3.1 and 3.2, the endothermic peaks at 78.83 and 855.04 °C on the DSC curve are caused by dehydration and fusion, respectively. As shown in Fig. 7, the diffraction peaks of Na_2CO_3 disappear at 700 °C. As shown in Fig. 6, obvious mass loss occurs as the temperature increases to above 700 °C. These results indicate that Na_2CO_3 has not fully decomposed at 700 °C. The disappearance of the Na_2CO_3 diffraction peaks at 700 °C can only be attributed to the conversion of the unreacted Na_2CO_3 into fusion state, but not decomposed completely. The TG curve in Fig. 6 shows that the mass loss begins to appear at 550 °C, suggesting that Na_2CO_3 has already started to decompose at 700 °C. However, no diffraction peak of the reaction product is observed in Fig. 7, indicating that the reaction products are also present in amorphous form. The amount of these amorphous substances, including reactants and products of the reaction, is significantly higher in the Na_2CO_3-Fe_2O_3 mixture than that in the Na_2CO_3-Al_2O_3 and Na_2CO_3-SiO_2 mixtures. At 1200 °C, the volatilization rate of sodium is 7.64%, which is also considerably higher than that in Na_2CO_3-Al_2O_3 and Na_2CO_3-SiO_2 mixtures. As the temperature increases to 850 °C, the diffraction peaks of $FeNaO_2$ appear, and its intensity becomes stronger at 950 °C. This result indicates that the amorphous substance crystallizes into $FeNaO_2$ gradually as the temperature increases from 850 °C to 950 °C. Amorphous substances are intermediate products of the reaction. The evaporation ratio increases with increasing amorphous substance amount. This result is probably due to the fact that the structural stability of these amorphous substances is lower than that of crystal substances, rendering these amorphous substances volatile.

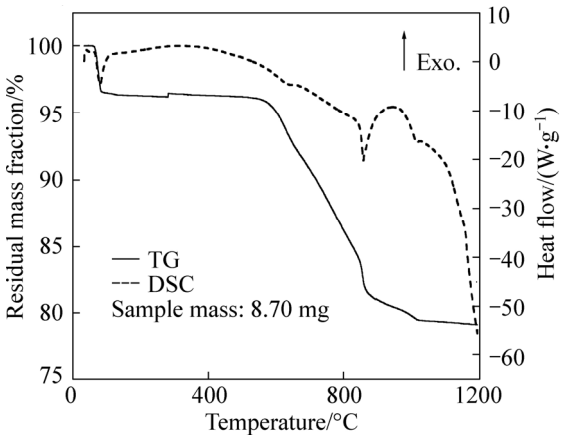

Fig. 6 TG and DSC curves of Na_2CO_3-Fe_2O_3 mixture

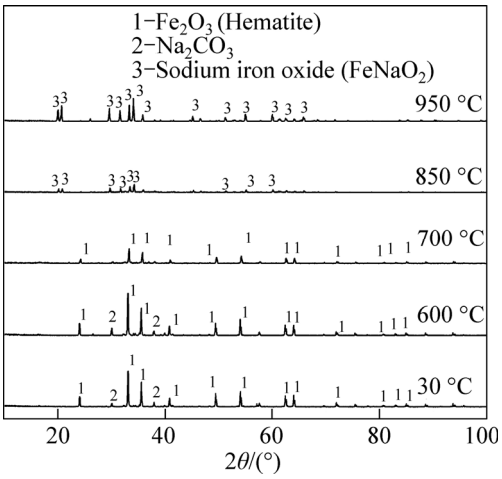

Fig. 7 XRD patterns of heated products of Na_2CO_3-Fe_2O_3 mixture

4 Conclusions

1) The most significant influence factor of ferric bauxite on sodium carbonate volatilization in direct reduction system is its iron content.

2) The volatilization of sodium is ascribed to the instability of amorphous intermediate-product. These amorphous substances are volatile, thus, the volatilization rate of sodium increases with its generating rate.

References

[1] HU Wen-tao, WANG Hua-Jun, LIU Xin-wei, SUN Chuan-yao. Correlation between aggregation structure and tailing mineral crystallinity [J]. International Journal of Minerals, Metallurgy and Materials, 2014, 21(9): 845−850.

[2] HU Wen-tao, WANG Hua-jun, SUN Chuan-yao, JI Chun-ling, HE Yang, WANG Cui-ling. Alkali consumption mechanism on ferrous bauxite reduction process [J]. Journal of Central South University (Science and Technology), 2012, 43(5): 1595−1605. (in Chinese)

[3] HU Wen-tao, WANG Hua-jun, SUN Chuan-yao, HE Yang, JI

Chun-ling, WANG Cui-ling, YU Hong-dong. Mechanism of reaction between ferric bauxite and soda lime in reduction atmosphere [J]. Journal of Harbin Engineering University, 2013, 34(5): 662−668. (in Chinese)

[4] MOTZFELDT K. The thermal decomposition of sodium carbonate by the effusion method [J]. The Journal of Physical Chemistry, 1955, 59: 139−147.

[5] BI Shi-wen. Alumina production technology [M]. Beijing: Chemical Industry Press, 2006: 127−128, 238.

[6] NEWKIRK A E, ALIFERIS I. Drying and decomposition of sodium carbonate [J]. Analytical Chemistry, 1958, 30: 982−984.

[7] ALBWETINI A V P, SILVA J L, FREIRE V N, SANTOS R P, MARTINS J L, CAVADA B S, CADENA P G, ROLIM P J R, PIMENTEL M C B, MARTINEZ C R, PORTO A L F, LIMA FILHO J L. Immobilized invertase studies on glass-ceramic support from coal fly ashes [J]. Chemical Engineering Journal, 2013, 214: 91−96.

[8] MAATT R, HANN K, KONE T, CHIRON S. Oxidation of 2, 4, 6-trinitrotoluene in the presence of different iron-bearing minerals at neutral pH [J]. Chemical Engineering Journal, 2011, 174: 453−458.

[9] HU Wen-tao, WANG Hua-jun, LIU Xin-wei, SUN Chuan-yao. Effect of nonmetallic additives on iron grain grindability [J]. International Journal of Mineral Processing, 2013, 130(10): 108−113.

[10] WEI Xiao-fei, ZHANG Guo-ping, CAI Yong-bing, LI Ling, LI Hai-xia. The volatilization of trace elements during oxidative pyrolysis of a coal from an endemic arsenosis area in southwest Guizhou, China [J]. Journal of Analytical and Applied Pyrolysis, 2012, 98: 184−193.

[11] SANTOS R M, CEULEMANS P, GERVEN T V. Synthesis of pure aragonite by sonochemical mineral carbonation [J]. Chemical Engineering Research and Design, 2012, 90(6): 715−725.

[12] LIU Xin-wei, FENG Ya-li, LI Hao-ran. Thermal decomposition kinetics of magnesite from thermogravimetric data [J]. Journal of Thermal Analysis Calorimetry, 2012, 107: 407−412.

[13] TABAK A, YILMAZ N, EREN E, CAGLAR B, AFSIN B, SARIHAN A. Structural analysis of naproxen-intercalated bentonite (Unye) [J]. Chemical Engineering Journal, 2011, 174: 281−288.

[14] BERTOL C D, CRUZ A P, STULZER H K, MURAKAMI F S, SILVA M A S. Thermal decomposition kinetics and compatibility studies of primaquine under isothermal and non-isothermal conditions [J]. Journal of Thermal Analysis Calorimetry, 2010, 102(1): 187−192.

[15] ZONG Nan-fu, LIU Yang. Learning about the mechanism of carbon gasification by CO_2 from DSC and TG data [J]. Thermochimica Acta, 2012, 527(10): 22−26.

[16] ZHAO De-qing, DAI Ya, CHEN Ke-fu, SUN Yu-feng, YANG Fei, CHEN Kun-yan. Effect of potassium inorganic and organic salts on the pyrolysis kinetics of cigarette paper [J]. Journal of Analytical and Applied Pyrolysis, 2013, 102: 114−123.

(Edited by YANG Bing)